Uncommon conductivity of R–Mn–Al (R = Gd, Tb) ternary compounds

2001 J. Phys.: Condens. Matter 13 9421

(http://iopscience.iop.org/0953-8984/13/42/303)

INSTITUTE OF PHYSICS PUBLISHING JOURNAL OF PHYSICS: CONDENSED MATTER

J. Phys.: Condens. Matter **13** (2001) 9421–9431 PII: S0953-8984(01)21488-X

Uncommon conductivity of R–Mn–Al (R = Gd, Tb) ternary compounds

B Ya Kotur[1], A M Palasyuk[1], E Bauer[2], H Michor[2] and G Hilscher[2]

[1] Department of Inorganic Chemistry, Ivan Franko National University of Lviv, Kyryla & Mefodiya Str. 6, UA-79005 Lviv, Ukraine
[2] Institute of Experimental Physics, TU Wien, Wiedner Hauptstraße 8/10, A-1040 Wien, Austria

E-mail: bauer@xphys.tuwien.ac.at

Received 20 January 2001, in final form 31 July 2001
Published 5 October 2001
Online at stacks.iop.org/JPhysCM/13/9421

Abstract

Crystal structure investigations, electrical resistivity and magnetoresistance measurements were carried out for $GdMn_xAl_{12-x}$ ($2.6 \leqslant x \leqslant 6.1$), $TbMn_xAl_{12-x}$ ($2.3 \leqslant x \leqslant 7.2$) ($ThMn_{12}$ structure-type, space group $I4/mmm$) and $Gd_2Mn_xAl_{17-x}$ ($6.6 \leqslant x \leqslant 12.2$), $Tb_2Mn_xAl_{17-x}$ ($8.5 \leqslant x \leqslant 10.2$) ($Th_2Zn_{17}$ structure-type, space group R-$3m$) ternary compounds. These aluminides are characterized by either disordered or partially ordered distributions of Mn and Al atoms in the crystal structure. However, the RMn_xAl_{12-x} phases exhibit a fully ordered structure ($CeMn_4Al_8$ structure-type) at the 1:4:8 stoichiometry. A relation between the crystal structure and conductivity of the R–Mn–Al ternaries was evaluated. Hopping conductivity in terms of variable range-hopping was used to describe electrical transport below 150–200 K. The width of the hopping conductivity regime appears to be related to the atomic disorder of the crystal structure. The maximum range was detected for $Gd_2Mn_{9.5}Al_{7.5}$ (50–200 K). The magnetic state of rare earth atoms does not substantially influence this type of conductivity since the magnetoresistance is below 1% in a large temperature range ($T > 0.5$ K) and magnetic fields up to 12 T.

1. Introduction

Binary and ternary alloys containing rare earth (R) and 3d transition metals (T) have been the subject of intensive investigations during the last few decades [1, 2]. The significant interest is connected with the large variety of their physical properties. Some of them exhibit properties which are promising for technical applications. The Mn-containing alloys and compounds, however, have been less extensively investigated in comparison with those containing other 3d elements like Fe, Co and Ni [1, 2].

The R–Mn–Al phase diagrams were previously studied at 500 °C only for R = Eu, Yb in the whole concentration range [3, 4]. Other ternary systems were investigated mainly in the

Al-rich region for R = Sc [5], La [6] and Ce [7], or for a rare earth content up to 33.3 at.% for R = Y [8], Nd [9, 10], Gd, Tb, Dy, Ho, Er, Tm, Lu [9].

Felner and Nowik [11] investigated the RMn_4Al_8 ternary compounds and observed an ordered distribution of R, Mn and Al atoms in the $ThMn_{12}$-type structure at this composition with the $CeMn_4Al_8$-type structure. Furthermore, Felner [12] reported the existence of $ThMn_{12}$-type ternary compounds at 800–1000 °C for the composition RMn_6Al_6 for heavy R (R = Y, Gd, Tb, Dy, Ho, Er, Tm, Yb, Lu) and that the RMn_6Al_6 compounds with light R (R = La, Ce, Pr, Nd, Sm) crystallize in the rhombohedral Th_2Zn_{17}-type structure. Ternary compounds RMn_4Al_8 (R = Nd, Gd, Tb, Dy, Ho, Er, Tm, Lu) exhibiting the $CeMn_4Al_8$-type structure were also observed by Rykhal' [14]. He reported for the same R series about $R_2Mn_9Al_8$ ternary compounds with an ordered distribution of atoms in the Th_2Zn_{17}-type structure although lattice parameters of these compounds were not presented. The data of Felner and Nowik [11–13] indicated the possibility of homogeneity ranges for $ThMn_{12}$-type R–Mn–Al ternary compounds including RMn_4Al_8 and RMn_6Al_6 compositions while Rykhal' [9, 14] observed only fixed compositions of RMn_4Al_8 for these compounds. Also, for the Th_2Zn_{17}-type R–Mn–Al ternaries different compositions RMn_6Al_6 [12] and $R_2Mn_9Al_8$ [14] were reported which indicate the existence of a homogeneity range.

Mössbauer and magnetic susceptibility studies were performed on RMn_4Al_8 compounds [13] indicating that the Mn atoms carry a localized magnetic moment ($\sim 1\mu_B$) and arrange anti-ferromagnetically with respect to R when the rare earth sublattice orders. The Néel temperatures range between $T_N = 7$ K (for R = Nd) and $T_N = 28$ K (for R = Gd). However, a recent study of magnetic properties of RMn_4Al_8 and RMn_6Al_6 alloys by means of magnetic susceptibility [15], magnetization and the specific heat measurements [16–18] contradicted the incipient results of Felner and Nowik [13]. No magnetic moment was evaluated for Mn, and moreover, anomalies indicative of magnetic ordering were found above 1.5–2 K for RMn_4Al_8 (R = Y, La, Nd, Gd, Dy, Er) compounds [16–17], except for $PrMn_4Al_8$ where a λ-type anomaly marks the onset of long-range magnetic order at 14 K [16]. Furthermore, Duong *et al* [17] interpreted the field dependence of a Schottky-like anomaly in $GdMn_4Al_8$ in terms of a short-range order rather than in terms of long-range magnetic order. For $GdMn_6Al_6$, which also crystallizes in the $ThMn_{12}$-type structure, more than one crystallographic site is occupied by the Mn atoms. This leads to sharp changes in magnetic interactions and ordering was reported at $T_N = 36$ K, but already fields of the order of 0.1 T strongly change magnetization.

So far, there are no data in the literature concerning transport properties of $ThMn_{12}$-type structure R–Mn–Al phases. Their proper homogeneity ranges were not yet reported, either. Additionally, many fewer data exist on the crystal chemistry and physical properties of Th_2Zn_{17}-type structure R–Mn–Al phases in comparison with those for $ThMn_{12}$-type ternaries. This justifies further investigations of the R–Mn–Al ternary systems in order to clarify the mentioned discrepancies with respect to crystal chemistry. Besides, we intended to study the correlation between the distribution of atoms in the crystal structures of the ternary compounds and their transport properties.

2. Experimental details

Alloys were obtained by arc-melting of pieces of individual elements (not less than 99.9 wt.% pure) on a water-cooled copper hearth under purified argon. The alloys used for the investigation had less than 2% deviation from the initial mass of charge. The alloys were homogenized in evacuated quartz tubes at 600 °C for 720 h. After annealing, the alloys were quenched in cold water. Powder x-ray diffraction analysis was carried out using the Debye–Scherrer method with Cr Kα radiation. Microscopic examination of some alloys on

an NEOPHOT-30 microscope was also carried out. The lattice parameters of the investigated compounds were determined by a least-squares refinement from DRON-2.0 (Fe Kα radiation), DRON-3M (Cu Kα radiation) and HZG-4a (Cu Kα radiation) powder diffractometer data. CSD [19] and DBWS-9006 [20] software were used for refinements of the crystal structure.

Resistivity and magnetoresistance measurements were performed on bar-shaped samples from 4 K, and partly from 0.5 K to room temperature and fields up to 12 T using a four-probe technique.

3. Results and discussion

3.1. $ThMn_{12}$-type compounds

The present systematic investigatigations of the (Gd, Tb)–Mn–Al ternary phases confirm the existence of RMn_4Al_8 compounds reported in [9, 11, 14]. These ternary compounds annealed at 600 °C exhibit wide homogeneity regions along the 7.7 at.% rare earth isoconcentrates: $GdMn_xAl_{12-x}$ ($2.6 \leqslant x \leqslant 6.1$) and $TbMn_xAl_{12-x}$ ($2.3 \leqslant x \leqslant 7.2$). These homogeneity ranges include two stoichiometries RMn_4Al_8 and RMn_6Al_6 for which Felner and Nowik [11, 12] observed the $ThMn_{12}$-type structure.

To illustrate the quality of the investigated samples crystallizing in the $ThMn_{12}$-type structure, x-ray data are collected in figures 1(a) and (b) for $TbMn_{7.2}Al_{4.8}$ and $GdMn_{4.04}Al_{7.96}$ as disordered and ordered members of these ternary phases. A least-squares fit to refine the data is indicated as a solid line and a difference pattern between both is shown on the lower panel of both figures, proving phase purity of the present samples. Some of the refined parameters are summarized in tables 1 and 2. As a result, full crystallographic order in the $ThMn_{12}$ structure is confirmed only at $x = 4$. For all other stoichiometries only a partially ordered distribution of the atoms occurs in the structure. For $x > 4$, Mn and Al atoms occupy statistically the 8*j* and 8*i* crystallographic sites and Mn atoms solely occupy the 8*f* site (see table 1). At $x \sim 4$ the structure approaches the ordered state, where 8*j* and 8*i* sites are occupied exclusively by Al and the 8*f* site by Mn atoms (see table 2). The observed splitting of some of the reflections as obvious from figure 1 originates from different c/a ratios (0.5710 for $TbMn_{7.2}Al_{4.8}$ and 0.5758 for $GdMn_{4.04}Al_{7.96}$).

Figure 2 displays the concentration-dependent lattice parameters and cell volumes within the homogeneity range of these series, revealing substantial deviations from linearity. The dashed lines in figure 2 are guides for the eyes and the error bar for each value measured is well below the symbol size. The significant decrease in the lattice constants of $GdMn_xAl_{12-x}$ and $TbMn_xAl_{12-x}$ with increasing x is connected with the substitution of larger Al atoms (metallic radius $r_{Al} = 0.143$ nm) by smaller Mn atoms ($r_{Mn} = 0.130$ nm) on the 8*i* and 8*j* sites.

3.2. Th_2Zn_{17}-type compounds

As an example for phases exhibiting the Th_2Zn_{17}-type structure x-ray patterns, the refinement of the data and the difference diagrams are displayed in figures 3(a) and (b) for $Tb_2Mn_9Al_8$ and $Tb_2Mn_{10.2}Al_{6.8}$. The homogeneity ranges of (Gd, Tb)–Mn–Al ternaries with the Th_2Zn_{17}-type structure are outlined in figure 4. Again, the error bar for each of the presented lattice parameters and unit cell volume is well below the symbol size. The dashed lines are guides for the eyes. The width of the respective homogeneity ranges decreases with increasing atomic number of the rare earth element. The variation in the lattice parameters appears to be non-linear for $Gd_2Mn_xAl_{17-x}$, but closely obeys Vegard's law for the Tb series.

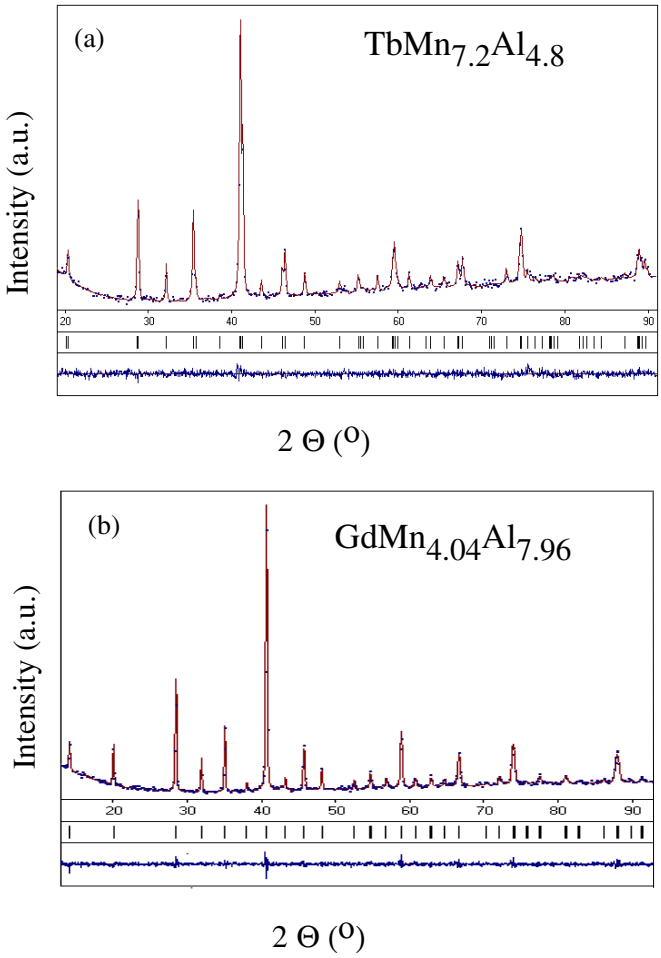

Figure 1. Observed (points), calculated by the Rietveld refinement (line) and difference (bottom) x-ray diffraction patterns of (a) $TbMn_{7.2}Al_{4.8}$ and (b) $GdMn_{4.04}Al_{7.96}$. The short vertical lines below the 2θ scale represent the positions of all possible Bragg reflections.

Table 1. Refined crystal structure, displacement (B_{iso}) parameters and site occupation (G) for $TbMn_{7.2}Mn_{4.8}$.[a]

Atom	Site	x/a	y/a	z/c	$B_{iso} \times 10^2$ (nm^2)	G
Gd	2*a*	0	0	0	0.69(7)	1.00 Gd
Mn	8*f*	1/4	1/4	1/4	0.74(10)	1.00 Mn
M2	8*i*	0.3514(10)	0	0	0.8(2)	0.60(1) Mn + 0.40(1) Al
M3	8*j*	0.2777(10)	1/2	0	1.2(3)	0.61(2) Mn + 0.39(2) Al

[a]DRON 3M powder diffractometer, Cu Kα-radiation, 2θ-range: 19°–91°, step width $2\theta = 0.05°$; $R_{(I)} = 0.09$; $ThMn_{12}$-type structure, space group $I4/mmm$; lattice parameters: $a = 0.882\,05(5)$ nm, $c = 0.503\,68(4)$ nm.

The distribution of atoms in the $Gd_2Mn_{10.3}Al_{6.7}$ and $Tb_2Mn_{10.2}Al_{6.8}$ ternaries is as follows: The 9*d* site is occupied by Mn atoms, while the three other sites (two 18*h* and 6*c*) are occupied by random mixtures of Mn and Al atoms of different ratios (tables 3 and 4). For another

Table 2. Refined crystal structure, displacement (B_{iso}) parameters and site occupation (G) for $GdMn_{4.04}Mn_{7.96}$.[a]

Atom	Site	x/a	y/a	z/c	$B_{iso} \times 10^2$ (nm^2)	G
Gd	2*a*	0	0	0	0.79(7)	1.00 Gd
M1	8*f*	1/4	1/4	1/4	0.29(10)	0.92(3) Mn + 0.08(3) Al
M2	8*i*	0.3487(10)	0	0	0.8(2)	0.03(1) Mn + 0.97(1) Al
M3	8*j*	0.2761(10)	1/2	0	1.1(3)	0.06(2) Mn + 0.94(2) Al

[a]DRON 3M powder diffractometer, Cu Kα-radiation, 2θ-range: 14°–93°, step width $2\theta = 0.05°$; $R_{(I)} = 0.05$; $ThMn_{12}$-type structure, space group $I4/mmm$; lattice parameters: $a = 0.888\,85(5)$ nm, $c = 0.511\,79(4)$ nm.

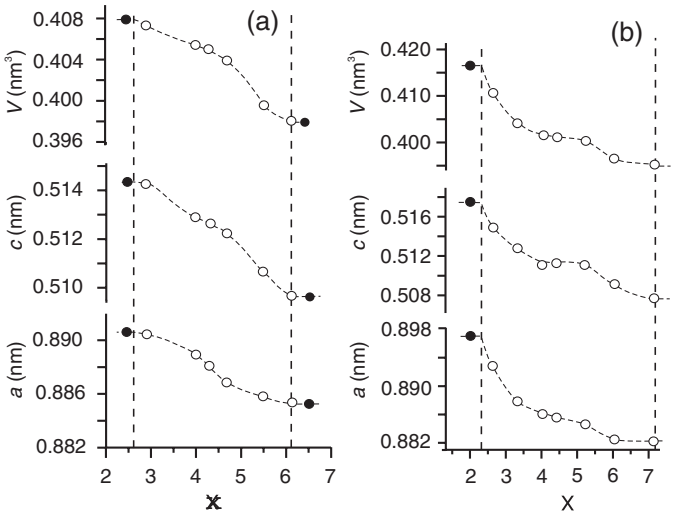

Figure 2. Lattice parameters (a, c) and cell volume (V) versus Mn content (x) for the RMn_xAl_{12-x} $ThMn_{12}$-type structure ternary compounds: (a) $GdMn_xAl_{12-x}$ ($2.6 \leqslant x \leqslant 6.1$); (b) $TbMn_xAl_{12-x}$ ($2.3 \leqslant x \leqslant 7.2$). Vertical dashed lines show the limits of the homogeneity ranges of the phases. Full and empty circles indicate multiphase and single phase samples, respectively.

stoichiometry, $Tb_2Mn_9Al_8$, the distribution of atoms is similar. Mn atoms prefer the 9*d* site, while the three other sites are randomly occupied by Mn and Al atoms (table 5). For none of the compositions investigated was an ordered distribution of atoms in the structure observed within the homogeneity range.

3.3. Physical properties

The temperature-dependent electrical resistivity was measured for a number of alloys within the homogeneity range for each of the (Gd, Tb)–Mn–Al ternary compounds with the $ThMn_{12}$- and Th_2Zn_{17}-structure. The particular composition of these alloys is given in table 6.

Among the $ThMn_{12}$-type compounds investigated, only the structurally ordered ones, i.e. $GdMn_4Al_8$ and $TbMn_4Al_8$, exhibit a metallic type of conductivity in the temperature range from 4.2 to 300 K (see figures 5(a) and (b)). The absolute resistivity values are of the order of several hundred $\mu\Omega$ cm, primarily provoked from microcracks and holes in the sample. All other $ThMn_{12}$-type structure samples show a shallow or fairly washed out minimum at

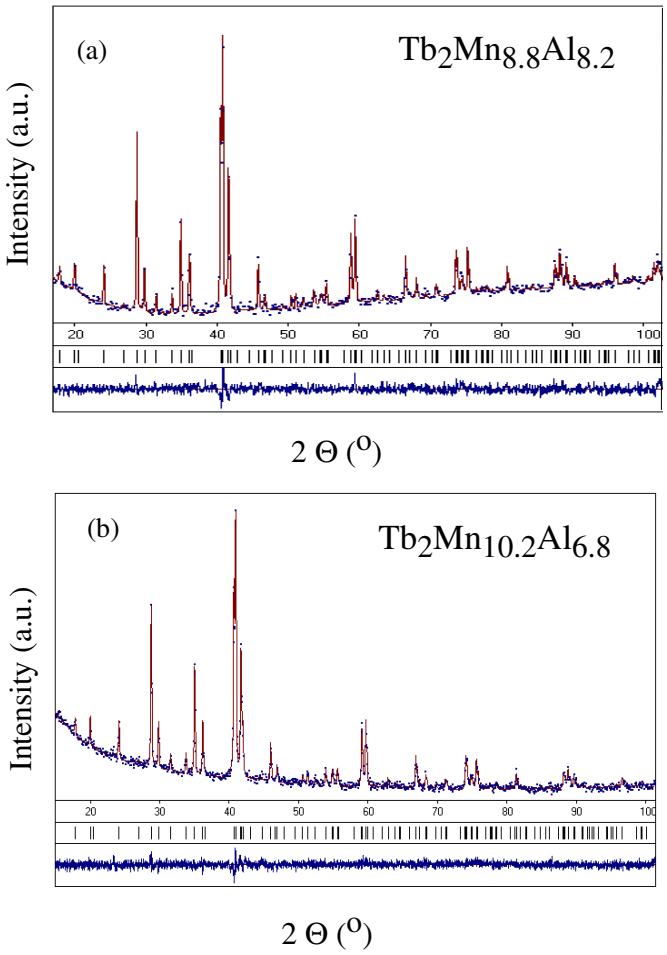

Figure 3. Observed (points), calculated by the Rietveld refinement (line) and difference (bottom) x-ray diffraction patterns of (a) $Tb_2Mn_9Al_8$ and (b) $Gd_2Mn_{10.2}Al_{6.8}$. The short vertical lines below the 2θ scale represent the positions of all possible Bragg reflections.

about 100 K and below this temperature the resistivity increases with decreasing temperature. Typical examples are presented in figures 5(c) and (d).

The resistivity of all $Gd_2Mn_xAl_{17-x}$ ($6.6 \leqslant x \leqslant 12.2$) and $Tb_2Mn_xAl_{17-x}$ ($8.5 \leqslant x$ 10.2) is characterized by a pronounced negative slope of $\rho(T)$ below room temperature. The $\rho(T)$ curves for some of these alloys are displayed in figures 6(a)–(d). The observed negative slope of $\rho(T)$, however, cannot be accounted for in terms of a simple activation-type behaviour, i.e. $\rho(T) = \rho_0 \cdot \exp(E_g/(2k_BT))$, where ρ_0 is a material-dependent constant and E_g is the gap in the electronic density of states at the Fermi energy. Rather, hopping conductivity in terms of variable range hopping (VRH) has been used for a description of the experimental data.

As is well known, overall resistivity increases considerably in disordered solids. Anderson [21] suggested that growing disorder can cause a localization of electrons, i.e. the wavefunction of those electrons, carrying the charge in the usual case, is no longer extended over the whole

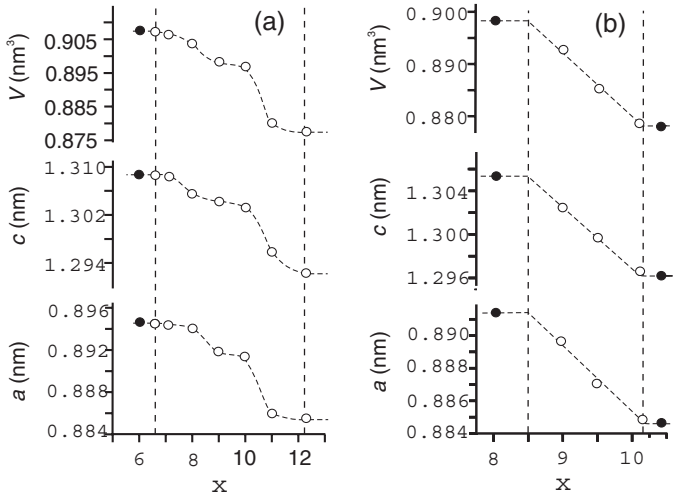

Figure 4. Lattice parameters (a, c) and cell volume (V) versus Mn content (x) for the $R_2Mn_xAl_{17-x}$ Th_2Zn_{12}-type structure ternary compounds: (a) $Gd_2Mn_xAl_{17-x}$ ($6.6 \leqslant x \leqslant 12.2$); (b) $Tb_2Mn_xAl_{17-x}$ ($8.5 \leqslant x \leqslant 10.2$). Vertical dashed lines show the limits of the homogeneity ranges of the phases. Full and empty circles indicate multiphase and single phase samples, respectively.

Table 3. Refined crystal structure, displacement (B_{iso}) parameters and site occupation (G) for $Gd_2Mn_{10.3}Al_{6.7}$.[a]

Atom	Site	x/a	y/a	z/c	$B_{iso} \times 10^2$ (nm)^2	G
Gd	6*c*	0	0	0.3412(4)	0.36(9)	1.00 Gd
M1	18*h*	0.5030(5)	1–x	0.1556(6)	0.8(2)	0.65(4) Mn + 0.35(4) Al
M2	18*h*	0.2945(10)	0	0	0.8(2)	0.41(4) Mn + 0.59(4) Al
M3	9*d*	1/2	0	1/2	0.3(2)	1.00 Mn
M4	6*c*	0	0	0.0989(10)	0.2(4)	0.47(4) Mn + 0.53(4) Al

[a]DRON 3M powder diffractometer, Cu Kα-radiation, 2θ-range: 15°–100°, step width $2\theta = 0.05°$; $R_{(I)} = 0.11$; Th_2Zn_{17}-type structure, space group R-3m; lattice parameters: $a = 0.891\,45(4)$ nm, $c = 1.304\,15(7)$ nm.

Table 4. Refined crystal structure, displacement (B_{iso}) parameters and site occupation (G) for $Tb_2Mn_{10.2}Al_{6.8}$.[a]

Atom	Site	x/a	y/a	z/c	$B_{iso} \times 10^2$ (nm^2)	G
Tb	6*c*	0	0	0.3412(4)	1.31(11)	1.00 Tb
M1	18*h*	0.5037(6)	1−x	0.1553(6)	1.3(2)	0.49(4) Mn + 0.51(4) Al
M2	18*f*	0.2923(9)	0	0	1.7(2)	0.47(4) Mn + 0.53(4) Al
M3	9*d*	1/2	0	1/2	1.5(2)	1.00 Mn
M4	6*c*	0	0	0.0967(8)	1.1(4)	0.71(4) Mn + 0.29(4) Al

[a]DRON 3M powder diffractometer, Cu Kα-radiation, 2θ-range: 15°–100°, step width $2\theta = 0.02°$; $R_{(I)} = 0.09$; Th_2Zn_{17}-type structure, space group R-3m; lattice parameters: $a = 0.885\,43(5)$ nm, $c = 1.297\,67(9)$ nm.

crystal, but is spatially confined in a very small region. This would mean that electrons at $T = 0$ cannot diffuse through the crystal; hence, the system behaves in an insulating manner. For $T > 0$, electrons may diffuse only by thermal activation due to phonons.

Table 5. Refined crystal structure, displacement (B_{iso}) parameters and site occupation (G) for $Tb_2Mn_9Al_8$.[a]

Atom	Site	x/a	y/a	z/c	$B_{iso} \times 10^2$ (nm^2)	G
Tb	6*c*	0	0	0.3420(2)	0.51(6)	1.00 Tb
M1	18*h*	0.5024(4)	1−x	0.1592(5)	1.3(2)	0.54(4) Mn + 0.46(4) Al
M2	18*f*	0.2906(6)	0	0	0.6(2)	0.33(4) Mn + 0.67(4) Al
M3	9*d*	1/2	0	1/2	0.8(2)	0.94(2) Mn + 0.06(2) Al
M4	6*c*	0	0	0.1018(2)	1.4(4)	0.57(3) Mn + 0.43(3) Al

[a]DRON 3M powder diffractometer, Cu Kα-radiation, 2θ-range: 15°–100°, step width $2\theta = 0.05°$; $R_{(I)} = 0.11$; Th_2Zn_{17}-type structure, space group R-3m; lattice parameters: $a = 0.889\,79(4)$ nm, $c = 1.301\,63(7)$ nm.

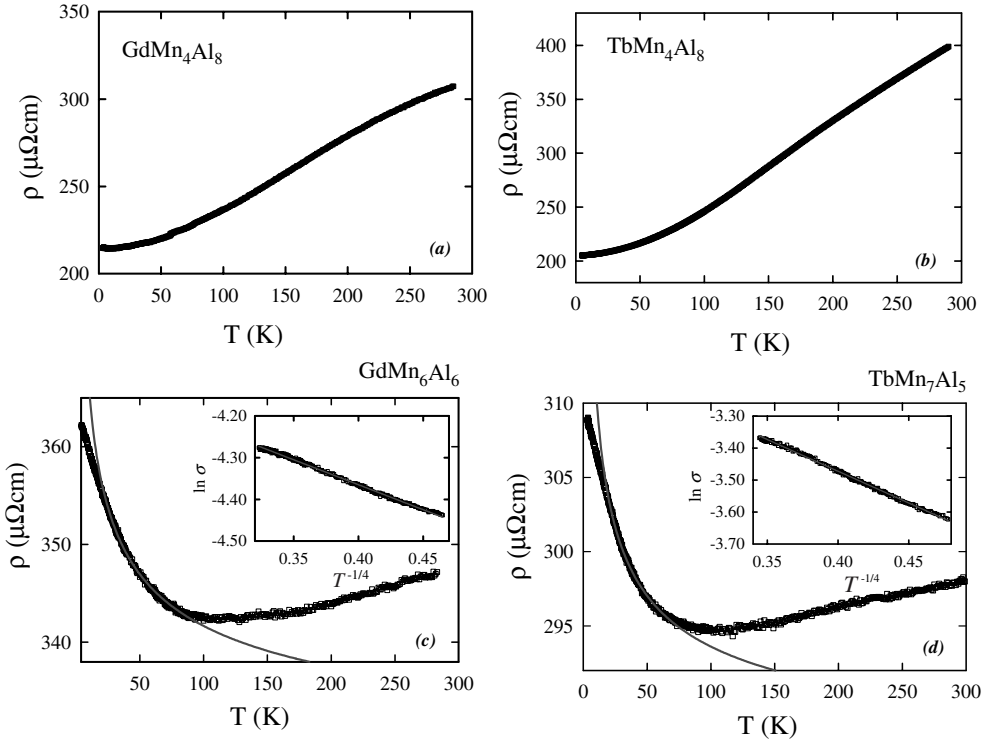

Figure 5. (a–d) Resistivity (ρ) versus temperature (T) for $ThMn_{12}$-type ternary compounds. The solid lines are least-squares fits, corresponding to equation (1).

In the three-dimensional case, the temperature-dependent hopping conductivity was derived by Mott [22] as

$$\sigma_{hc}(T) = \sigma_0 \exp(-A/T)^{1/4} \tag{1}$$

where σ_0 is a material constant and A corresponds to a characteristic temperature of the system. This model of hopping conductivity was used to characterize the low-temperature resistivity of all ternaries investigated except RMn_4Al_8 (R = Gd, Tb). In order to take into account the temperature-independent background contribution, the measured data are analysed according to $\rho = \rho_0 + \rho_{hc}$, with ρ_0 the residual resistivity and $\rho_{hc} = 1/\sigma_{hc}$. The temperature ranges described by hopping conductivity are presented in table 6. As can be seen from the solid lines

Table 6. Compositions of alloys for which the $\rho(T)$ measurements were done, the observed hopping conductivity temperature ranges (ΔT) and characteristic temperatures (T_o).

Composition	ΔT (K)	T_o (K)	Composition	ΔT (K)	T_o (K)
$GdMn_6Al_6$	20–80	16.5	$TbMn_7Al_5$	20–75	7
$GdMn_{4.6}Al_{7.4}$	4–15	9.9	$TbMn_{4.6}Al_{7.4}$	10–23	3.3
$GdMn_{4.2}Al_{7.8}$	4–15	3.2	$TbMn_{4.2}Al_{7.8}$	4–20	2.2
$GdMn_4Al_8$	–	–	$TbMn_4Al_8$	–	–
$GdMn_{3.9}Al_{8.1}$	5–15	1			
$Gd_2Mn_{10}Al_7$	60–150	54	$Tb_2Mn_{10}Al_7$	30–100	16
$Gd_2Mn_{9.5}Al_{7.5}$	50–200	27.5	$Tb_2Mn_{9.5}Al_{7.5}$	40–100	47
$Gd_2Mn_7Al_{10}$	70–190	21	$Tb_2Mn_{8.8}Al_{8.2}$	80–150	17

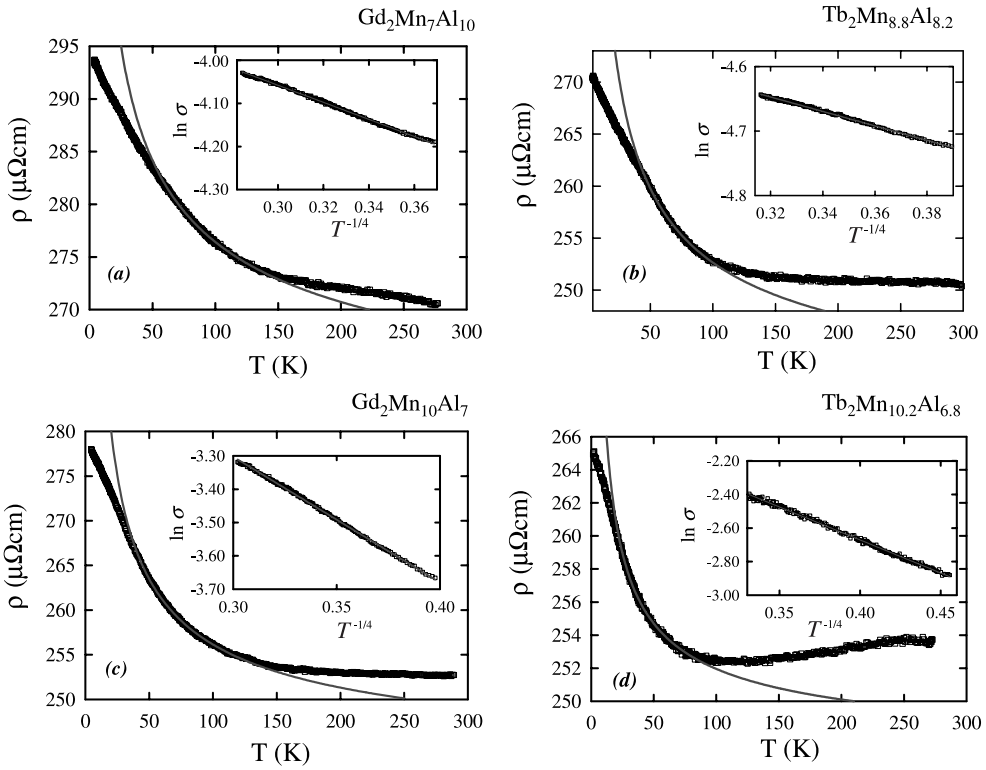

Figure 6. (a–d) Resistivity (ρ) versus temperature (T) for Th_2Zn_{17}-type ternary compounds. The solid lines are least-squares fits, corresponding to equation (1).

in figures 5 and 6 the experimental data at low temperatures are satisfactorily described in terms of the VRH model, equation (1). A convincing method to graphically express hopping conductivity in these compounds is to plot σ on a logarithmic scale versus $T^{-1/4}$. In the case that equation (1) appropriately accounts for the physics of the disordered 1:12 and 2:17 compounds, resistivity should behave linearly in such a plot. In fact, the insets in figures 5 and 6 nicely demonstrate the unusual transport processes in a metallic state.

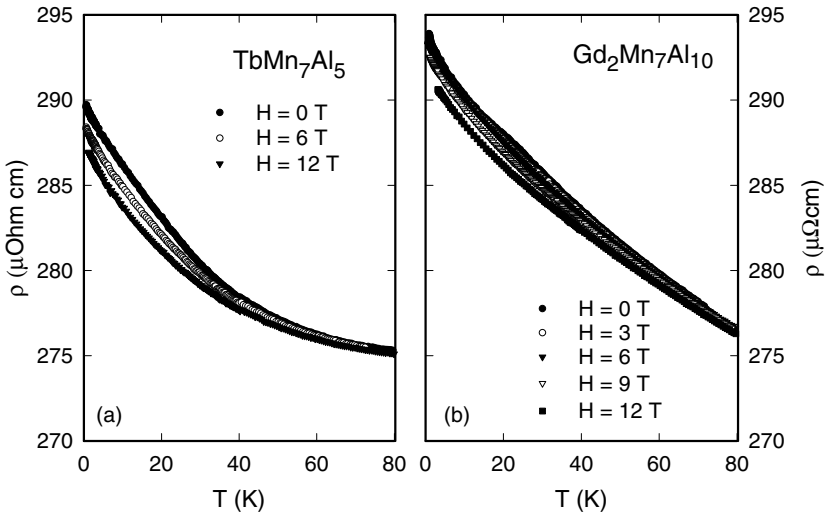

Figure 7. Temperature- and field-dependent resistivity (ρ) of (a) $TbMn_7Al_5$ and (b) $Gd_2Mn_7Al_{10}$.

According to figure 5 and table 6 the width of the hopping conductivity range is reduced when the composition of the alloy is close to the stoichiometry RMn_4Al_8 (4–15 K for $GdMn_{4.2}Al_{7.8}$, $GdMn_{4.6}Al_{7.4}$ and 4–20 K for $TbMn_{4.2}Al_{7.8}$, see table 6). Growing disorder due to the solid solution leads to an extension of this range up to 20–75 K for $TbMn_7Al_5$ and up to 20–80 K for $GdMn_6Al_6$ (see figure 5). It should be emphasized that the temperature range of hopping conductivity for the series $R_2Mn_xAl_{17-x}$ (R = Gd, Tb) is distinctly larger in comparison with that for $ThMn_{12}$-type compounds. We may therefore conclude that the range for hopping conductivity is proportional to the atomic disorder in the crystal structure.

The field-dependent resistivity of the two phases of the investigated series is shown in figures 7(a) and (b) for fields up to 12 T. As is obvious from these data, magnetic fields do not significantly change the overall resistivity behaviour. In both cases, and in general for all the Gd–Mn–Al and Tb–Mn–Al samples, the magnetoresistance does not exceed values of about 1% at the lowest temperatures. Although the magnetoresistance is negative, indicating some quenching of magnetic fluctuations, the very small changes of resistivity in reasonably large fields exclude magnetic scattering processes as the principal interaction mechanism in these series of compounds. Moreover, hopping conductivity is not significantly influenced by external magnetic fields. Preliminary studies on phases based on Y and Sc are also characterized by VRH over some extended temperature range. As a consequence of these particular observations, we may conclude that Mn in these ternaries is primarily responsible for the quite unusual transport observed.

Investigations of magnetic properties and of the specific heat of both series are in progress in order to understand the magnetic behaviour of these ternaries. Examinations of the temperature-dependent electrical resistivity as well as other physical properties on different R–Mn–Al and R–Fe–Al ternaries are also in progress in order to get more insight into the nature of transport in such systems and to settle the question whether hopping conductivity occurs exclusively in the R–Mn–Al ternaries or if it occurs in a larger group of disordered ternary rare earth intermetallics.

Acknowledgments

The authors are grateful to the Austrian Cooperation Bureau for financial support. Parts of the work were supported by the Austrian FWF, project P 12899.

References

[1] Suski W 1996 *Handbook on the Physics and Chemistry of Rare Earths* vol 22 ed K A Gschneidner Jr and L Eyring (Amsterdam: Elsevier) pp 143–294
[2] Li H S and Coey J M D 1991 *Handbook of Magnetic Materials* vol 6 ed K H J Buschow (Amsterdam: Elsevier) pp 1–83
[3] Manyako N B, Yanson T I and Zarechnyuk O S 1988 *Izv. AN SSSR, Met.* **5** 212
[4] Yanson T I, Manyako N B, Bodak O I, Cerny R, Gladyshevskii R E and Yvon K 1995 *J. Alloy Compd.* **219** 219
[5] Dritz M E, Toropova L S and Guschina F L 1984 *Izv. AN SSSR, Met.* **6** 221
[6] Emes-Misenko O Y 1972 *Visnyk Lviv. Univ., Ser. Khim.* **12** 12
[7] Zarechnyuk O S, Kolobnyov I F and Teslyuk M Yu 1983 *Zh. Neorg. Khim.* **8** 1668
[8] Rykhal' R M, Zarechnyuk O S and German N V 1971 *Izv. AN SSSR, Met.* **6** 205
[9] Rykhal' R M 1995 *Nauk.-pract. Conf. Lvivski Khim. Chytannya, Lviv Abstracts* p 82
[10] Zarechnyuk O S and Frankevich D P 1987 *Dokl. AN Ukr. SSR* **4** 82
[11] Felner I and Nowik I 1978 *J. Phys. Chem. Solids.* **39** 951
[12] Felner I 1980 *J. Less-Common Metals* **72** 241
[13] Felner I and Nowik I 1979 *J. Phys. Chem. Solids* **40** 1035
[14] Rykhal' R 1983 *Chetvyortaya Vsesoyuznaya Conf. po Kristallokhimii Intermetallicheskih Soedinenij, Lvov Abstracts* p 24
[15] Coldea M, Neumann M, Lütkehoff St, Mähl S and Coldea R 1998 *J. Alloy. Compound* **278** 72
[16] Hagmusa I H, Klaasse J C P, Brük E, de Boer F R and Buschow K H J 2000 *J. Alloy. Compound* **297** 21
[17] Duong N P, Klaasse J C P, Brük E, Hagmusa I H, de Boer F R and Buschow K H J 2000 *J. Alloy. Compound* **309** L10
[18] Duong N P, Klaasse J C P, Brük E, Hagmusa I H, de Boer F R and Buschow K H J 2001 *J. Alloy. Compound* **315** 28
[19] Akselrud L G, Grin Yu N, Zavalii P Yu, Pecharsky V K and Fundamensky V S 1989 *12th Eur. Crystallogr. Meeting (Moscow) Abstracts* vol 3 p 155
[20] Wiles D B and Young R A 1981 *J. Appl. Crystallogr.* **14** 149
[21] Anderson P W 1958 *Phys. Rev.* **109** 1492
[22] Mott N F 1970 *Phil. Mag.* **22** 7